Electronic Properties and Phase Transformations in $CoMoO_4$ and $NiMoO_4$: XANES and Time-Resolved Synchrotron XRD Studies

José A. Rodriguez,* Sanjay Chaturvedi, and Jonathan C. Hanson

Department of Chemistry, Brookhaven National Laboratory, Upton, New York 11973

Alberto Albornoz and Joaquín L. Brito*

Centro de Química, Instituto Venezolano de Investigaciones Científicas (IVIC) Caracas 1020-A, Venezuela

Received: July 2, 1997; In Final Form: September 22, 1997

The thermal stability of a series of cobalt and nickel molybdates ($AMoO_4 \cdot nH_2O$, α-$AMoO_4$, and β-$AMoO_4$; A = Co or Ni) was examined using synchrotron-based time-resolved X-ray powder diffraction (XRD). The results of X-ray absorption near-edge spectroscopy (XANES) indicate that the Co and Ni atoms are in octahedral sites in all these compounds, while the coordination of Mo varies from octahedral in the α-phases to tetrahedral in the β-phases and hydrates. Upon heating of $AMoO_4 \cdot nH_2O$, evolution of gaseous water was seen at two different temperature ranges: 100−200 °C for reversibly bound H_2O; 200−400 °C for H_2O from the crystal structure. The results of time-resolved XRD show a direct transformation of the hydrates into the β-$AMoO_4$ compounds (following a kinetics of first order) without any intermediate phase. This is probably facilitated by the similarities that $AMoO_4 \cdot nH_2O$ and β-$AMoO_4$ have in their structural and electronic properties. The XRD experiments show that the α-$AMoO_4 \rightarrow$ β-$AMoO_4$ transitions occur at much higher temperatures than the hydrate $\rightarrow$ β-$AMoO_4$ transformations ($\Delta T \approx 150$ °C in $CoMoO_4$ and 280 °C in $NiMoO_4$). The activation energy for the α-$NiMoO_4 \rightarrow$ β-$NiMoO_4$ transition is ∼40 kcal/mol larger than that for the $NiMoO_4 \cdot nH_2O \rightarrow$ β-$NiMoO_4 + nH_2O$ reaction. The larger activation energy reflects the change in the coordination of Mo ($O_h \rightarrow T_d$) that occurs during the α → β transition. The K- and L-edges of Co in XANES spectra indicate that there are no big variations in the electronic properties of this metal when comparing $CoMoO_4 \cdot nH_2O$, α-$CoMoO_4$, and β-$CoMoO_4$. The same is valid for the electronic properties of Ni in the nickel molybdates. In contrast, the $L_{2,3}$-edges of Mo show large changes in the splitting of the Mo 4d orbitals as the coordination of this metal varies from octahedral (α-phases) to tetrahedral (β-phases and hydrates). The features near the threshold in the O K-edge spectra track very well the splitting of the Mo 4d orbitals in tetrahedral and octahedral fields and can be very useful for probing the local symmetry of Mo atoms in molybdenum oxides.

I. Introduction

Cobalt and nickel molybdates constitute an interesting group of compounds because of their structural, electronic, and catalytic properties.[1−16] The molybdates may be prepared by reacting MoO_3 with cobalt or nickel oxides at high temperature ($CoMoO_4$ and $NiMoO_4$ formation),[17] or by precipitation from aqueous solution of soluble salts ($H_2O-CoMoO_4$ and $H_2O-NiMoO_4$ formation).[5,7,18] At atmospheric pressure, two phases, usually designated as α and β, are known of $CoMoO_4$ and $NiMoO_4$.[1−3] The main difference between them is in the coordination of the Mo^{6+} ions, octahedral in the α-phase and tetrahedral in the β-phase. In both isomorphs, the Co^{2+} or Ni^{2+} ions occupy sites with octahedral coordination. The structures of the $H_2O-CoMoO_4$ and $H_2O-NiMoO_4$ compounds are unknown. Measurements of differential thermal analysis (DTA) suggest that in these systems the metal cations have a coordination similar to that seen in the β-phase of $CoMoO_4$ and $NiMoO_4$.[7,16]

Cobalt and nickel molybdates are important components of industrial catalysts for the partial oxidation of hydrocarbons.[8] Molybdates of the type $AMoO_4$ (A = Co or Ni) have been detected several times[11,20] in industrial $Co(Ni)-Mo/Al_2O_3$ catalysts used in hydrodesulfurization processes. The catalytic properties of the cobalt and nickel molybdates are closely related to their structures. The β-phase of $NiMoO_4$ is almost twice as selective for the dehydrogenation of propane to propene than the α-phase.[15] In a series of studies,[5,7,19] the sulfided $H_2O-CoMoO_4$ and $H_2O-NiMoO_4$ compounds were found to be much better catalysts for the hydrodesulfurization (HDS) of thiophene than the corresponding sulfided α- and β-isomorphs. The HDS activity of these systems increased in the following order: α < β < hydrate.[7] On the basis of these results, we decided to carry out a detailed study of the phase transformations and electronic properties of cobalt and nickel molybdates using synchrotron-based X-ray powder diffraction (XRD) and X-ray absorption near-edge spectroscopy (XANES).

Recent works have shown that the local site symmetry of molybdenum oxide phases dispersed on MgO, TiO_2, Al_2O_3, and SiO_2 can be determined using XANES at the Mo $L_{2,3}$-edges.[4,21] This spectroscopy probes 2p → 4d electronic transitions, and the variable splitting in the Mo $L_{2,3}$-edges reflects the ligand field splitting of the d orbitals.[4,22] In a tetrahedral coordination the splitting of the Mo 4d orbitals is smaller than the splitting in an octahedral coordination.[4,22] On the other hand, it is well-known that the O K-edge XANES features can be used to distinguish oxygen atoms under different bonding

* Corresponding authors.

S1089-5647(97)02137-8 CCC: $15.00
Published on Web 01/28/1998

environments.[23−25] For transition metal oxides a direct relationship has been found between the features in the O K-edge spectrum and the number of d electrons in the metal.[23,26] Thus, a study of the Mo $L_{2,3}$-edges and O K-edges can give simultaneous information about the structural and electronic properties of the cobalt and nickel molybdates and provide spectra that can be used as "fingerprints" to detect the presence of these compounds in supported catalysts.

Investigations at Brookhaven National Laboratory have recently established the feasibility of conducting subminute, time-resolved XRD experiments under a wide variety of temperature and pressure conditions (−190 °C < T < 900 °C; $P \leq 45$ atm).[27] This important advance results from combining the high intensity of synchrotron radiation with rapid new parallel data-collection devices.[27] Using this unique approach we monitored the changes that occur in the $H_2O-AMoO_4$, α-$AMoO_4$, and β-$AMoO_4$ systems as a function of temperature.

II. Experimental Section

II.1. Preparation of the Molybdates. A series of H_2O-$AMoO_4$ and $AMoO_4$ samples was prepared following the methodology described in detail in refs 5 and 7. Hydrated compounds of general formula $AMoO_4 \cdot nH_2O$ were synthesized by coprecipitation from aqueous solutions of A^{2+} salts (nickel or cobalt nitrates) and ammonium heptamolybdate.[7,18] The α-phase of the molybdates was prepared by firing at 550 °C the corresponding $H_2O-AMoO_4$ compounds and cooling slowly to room temperature (∼5 °C/min). This produced directly the α-$NiMoO_4$ isomorph.[5,6] In the case of α-$CoMoO_4$, thorough grinding of the calcined product was necessary to complete the transformation, as the β phase of this molybdate can be quenched at room temperature.[7] The β-$CoMoO_4$ isomorph was prepared by calcining the $H_2O-CoMoO_4$ precursor at 550 °C, followed by fast cooling (∼100 °C/min) to room temperature. Finally, the standard preparation of β-$NiMoO_4$ consisted of calcination of the $H_2O-NiMoO_4$ precursor at 550 °C and cooling to the temperature required for further work (always above 300 °C).

II.2. Thermal Desorption. The desorption of water from the $H_2O-AMoO_4$ compounds as a function of temperature was monitored using a RXM-100 instrument from Advanced Scientific Designs. Usually the temperature of the sample was raised from 40 to 600 °C at heating rates of 10−30 °C/min. Pure helium was used as the carrier gas with a flow rate of 80 mL/min. Chemical analysis of the desorbing gases was made by means of a quadrupole mass spectrometer (UTI-100C).

II.3. Time-Resolved X-ray Powder Diffraction. The time-resolved diffraction data were collected on beamline X7B of the National Synchrotron Light Source (NSLS) at Brookhaven National Laboratory (BNL). The optics of the beamline is described elsewhere.[28] The sample was kept in a quartz capillary sealed with glue. The capillary was placed on a goniometer and the sample was heated using a small resistance heater placed under the capillary.[27] A chromel−alumel thermocouple was used to measure the temperature of the sample. The accuracy of the thermocouple readings was verified by doing blank runs with silver powder and checking against the known changes in the cell parameters of this metal as a function of temperature.[27] Data collections were performed using wavelengths of 0.957 and 1.116 Å. The X-ray powder patterns were accumulated on a flat image plate (IP) detector. The IP is mounted on a computer-controlled translating slide and moves behind a vertical steel slit with a horizontal opening of 3 mm. A continuous series of powder patterns can be obtained where the time (or temperature) resolution is defined by the translation speed of the IP detector combined with the width of the vertical slit.[29] Knowing the starting and ending values of the experimental variable (time in isothermal experiments; temperature and heating rate in dynamic experiments), the setting of each powder pattern is unequivocally determined.[29] The images collected on the IP were retrieved using a Fuji BAS2000 scanner.

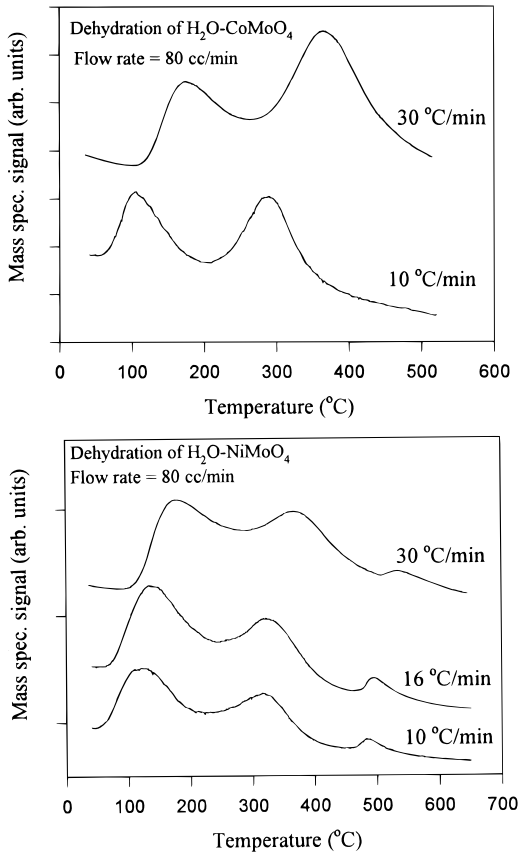

Figure 1. H_2O-thermal desorption spectra for $H_2O-CoMoO_4$ and $H_2O-NiMoO_4$ at heating rates of 10, 16, and 30 °C/min. Pure helium was used as the carrier gas at a flow rate of 80 mL/min. The spectra were acquired monitoring mass 18.

II.4. X-ray Absorption Near-Edge Spectroscopy. The Mo $L_{2,3}$-edge XANES spectra were recorded at the NSLS on beamline X19A. The X-ray photons were monochromatized using a NSLS boomerang-type flat crystal monochromator with Si(111) crystals. The energy resolution at the Mo L-edges was ∼0.5 eV. The harmonic content was reduced by detuning the monochromator crystals by ∼90%. The Mo $L_{2,3}$-edge spectra were measured in the "fluorescence-yield mode" using a Stern-Heald-Lytle detector with argon as the detector gas.[30]

The O K-edge and L-edges of Co and Ni were studied at beamline U7A of the NSLS. This beamline is equipped with a toroidal−spherical grating monochromator. The energy resolution at the O K-edge was close to 0.5 eV. For the Co and Ni $L_{2,3}$-edges the energy resolution was in the range of 0.5−0.8 eV. The O K-edge and Co and Ni $L_{2,3}$-edge spectra were recorded in the "electron-yield mode" by using a channeltron multiplier located near the sample surface.[31] All the XANES spectra were acquired at room temperature.

III. Results

III.1. Dehydration of $H_2O-CoMoO_4$ and $H_2O-NiMoO_4$. Figure 1 shows H_2O-thermal desorption spectra for H_2O-

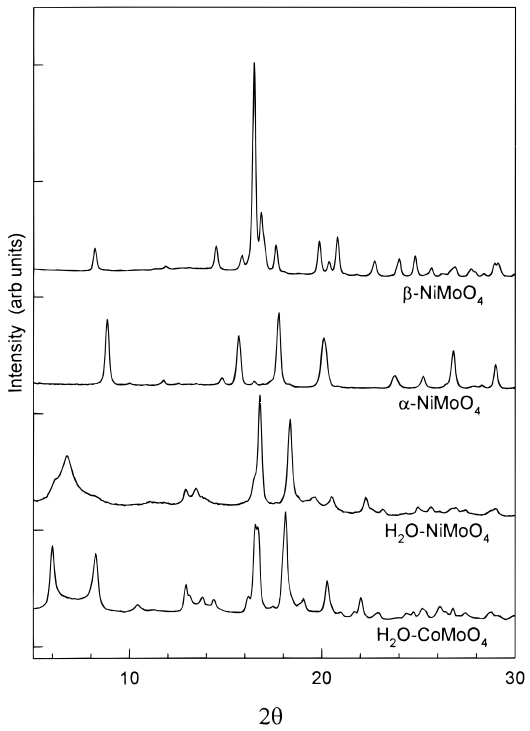

Figure 2. X-ray powder diffraction patterns for $H_2O-CoMoO_4$, $H_2O-NiMoO_4$, α-$NiMoO_4$, and β-$NiMoO_4$. For the first three compounds, the patterns were acquired at room temperature. In the case of β-$NiMoO_4$, the pattern was taken after heating a $H_2O-NiMoO_4$ sample to 550 °C. The XRD data were recorded using a wavelength of 0.957 Å.

$CoMoO_4$ and $H_2O-NiMoO_4$ at heating rates that vary from 10 to 30 °C/min. In these experiments we did not find any evidence for the desorption of ammonia (a species that could be present in the samples due to the procedure used to synthesize them[5−7]). Masses 17 and 16 tracked the line shape of mass 18, and their relative intensities were consistent with the cracking pattern for H_2O in our mass spectrometer. In Figure 1, the water desorption temperatures depend strongly on the heating rate. For both compounds one sees two large desorption peaks at temperatures below 500 °C. In the case of $H_2O-NiMoO_4$, there is an additional, small desorption peak at 490−520 °C that was not seen after heating $H_2O-CoMoO_4$ samples up to 650 °C. At a heating rate of 10 °C/min, the temperatures at which water evolves from $H_2O-CoMoO_4$ are ∼40 °C smaller than those seen for the evolution of the molecule from $H_2O-NiMoO_4$. This difference becomes negligible when the heating rate is increased to 30 °C/min. It is likely that at this high heating rate the position of the peaks in the H_2O-TDS spectra is strongly affected by the rate at which gaseous water can be removed from the reaction cell. Independently of the heating rate, there are significant differences in the relative intensities of the water desorption peaks. For $H_2O-NiMoO_4$, the feature at 110−190 °C is the most intense in the desorption spectrum. On the other hand, in the case of $H_2O-CoMoO_4$, the dominant water desorption peak appears at 300−380 °C.

Figure 2 displays X-ray powder diffraction patterns for the $H_2O-AMoO4$ compounds at room temperature. In general, the XRD results are similar to JCPDS Powder Diffraction File Cards reported for hydrates of $CoMoO_4$ (card 26−477) and $NiMoO_4$ (card 13−128).[32] From these data, it is clear that there are important variations in the powder patterns of these compounds. The crystal structures of $H_2O-CoMoO_4$ and $H_2O-NiMoO_4$ are probably different. Thus, it is not surprising that their H_2O-TDS spectra are also different. In Figure 2, we also show typical

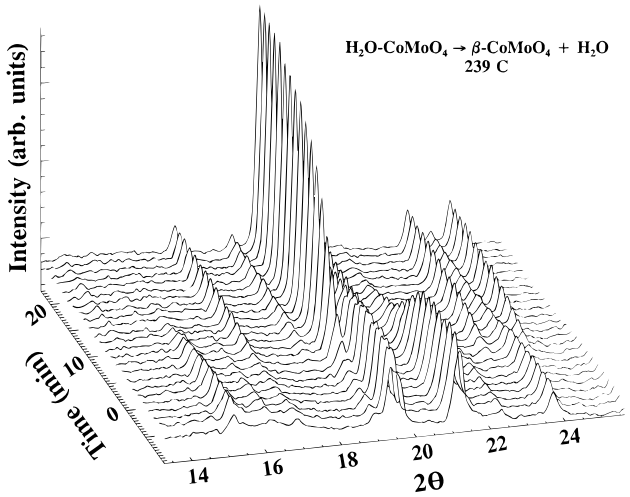

Figure 3. Time-resolved X-ray powder diffraction patterns for the dehydration of $H_2O-CoMoO_4$. At time "0" the sample reached 239 °C and was held at this temperature for 30 min. The XRD experiments were carried out using a wavelength of 1.116 Å.

powder patterns for the α- and β-phases of $AMoO_4$ compounds. These patterns agree very well with the corresponding JCPDS Powder Diffraction File Cards (21-868, 25-1434, and 33-948).[32] It is obvious that there are large differences in the XRD patterns of the $H_2O-AMoO_4$, α-$AMoO_4$, and β-$AMoO_4$ systems.

Using time-resolved XRD, we monitored the changes that occur in $H_2O-CoMoO_4$ and $H_2O-NiMoO_4$ when the temperature is increased from 25 to 600 °C. Previous studies report that at 330[33a] and 880 °C,[33b] $H_2O-CoMoO_4$ loses water and transforms into β-$CoMoO_4$. Our XRD results for the heating of $H_2O-CoMoO_4$ ($\Delta T = 5$ °C/min) show that the lines for this compound start to disappear around 200 °C, and simultaneously lines for the corresponding β-isomorph begin to appear. A typical result for this transformation is shown in Figure 3. No change in the diffraction pattern was observed at temperatures below 200 °C. This indicates that the first water desorption peak that $H_2O-CoMoO_4$ exhibits in Figure 1 is associated with reversibly bound molecules (i.e., water molecules that do not form part of the compound crystal structure). At the onset of the second water desorption peak, the crystal structure of the hydrate begins to collapse and β-$CoMoO_4$ appears.

Following experiments similar to those seen in Figure 3, one can get the rate for the disappearance of $H_2O-CoMoO_4$, or appearance of β-$CoMoO_4$, under isothermal conditions. We did this at temperatures of 214, 224, and 239 °C, focusing our attention on the 2θ line that appears at 21° in the powder pattern for $H_2O-CoMoO_4$. This line is one of the main lines of the hydrate and does not overlap with lines of the β-isomorph. The top panel in Figure 4 shows how the logarithm of the intensity of the 21° line changes with time at temperatures of 214 and 224 °C. The linear relationship between $\ln(I/I_o)$ and time indicates that the dehydration of $H_2O-CoMoO_4$ follows a kinetics of first-order with rate constants of 0.079 and 0.180 min^{-1} at 214 and 224 °C, respectively. The corresponding Arrhenius plot at the bottom of Figure 4 gives an apparent activation energy of 27.6 kcal/mol and a preexponential factor of 2.217×10^{11} min^{-1} for the dehydration process.

It is known that β-$NiMoO_4$ can be obtained by heating $H_2O-NiMoO_4$[7] and $NiMoO_4 \cdot mH_2O \cdot nNH_3$ precursors[34] at 500 °C. Using time-resolved XRD, we monitored the reaction $H_2O-NiMoO_4 \rightarrow \beta$-$NiMoO_4 + H_2O$, under isothermal conditions (Figure 5) or raising the temperature of the sample from 40 to

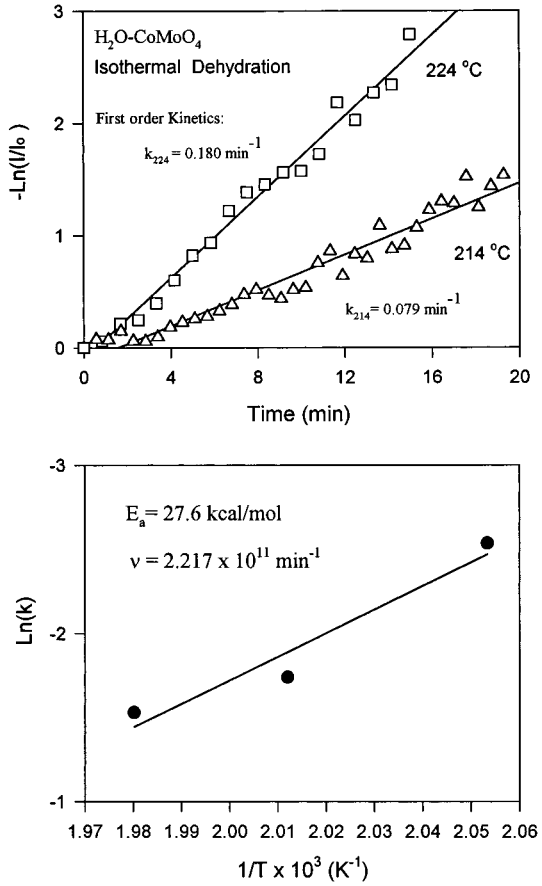

Figure 4. Top panel: Logarithm of the concentration of $H_2O-CoMoO_4$ as a function of time at 214 and 224 °C. The concentration of $H_2O-CoMoO_4$ was assumed to be proportional to the intensity of the 2θ line at 21° in the XRD pattern ($\lambda = 1.116$ Å). Bottom panel: Arrhenius plot for the transformation of $H_2O-CoMoO_4$ into β-$CoMoO_4$.

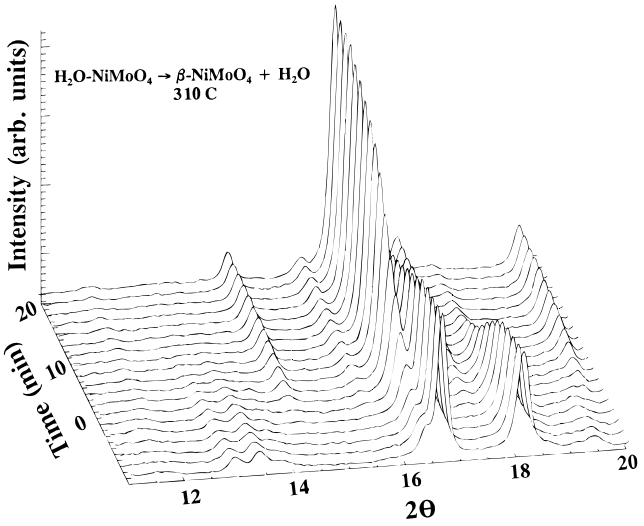

Figure 5. Time-resolved X-ray powder diffraction patterns for the dehydration of $H_2O-NiMoO_4$. At time "0" the sample reached 310 °C and was held at this temperature for 30 min. The XRD experiments were carried out using a wavelength of 0.957 Å.

600 °C at heating rates of 5−15 °C. No change in the diffraction pattern of the $H_2O-NiMoO_4$ samples was observed at temperatures below 250 °C. The rate of the hydrate to β-isomorph transformation was relatively fast around 320 °C, and at 400 °C only the characteristic lines of β-$NiMoO_4$ were seen in the powder diffraction patterns. Further heating from 400 to 600 °C did not produce any change in the XRD patterns.

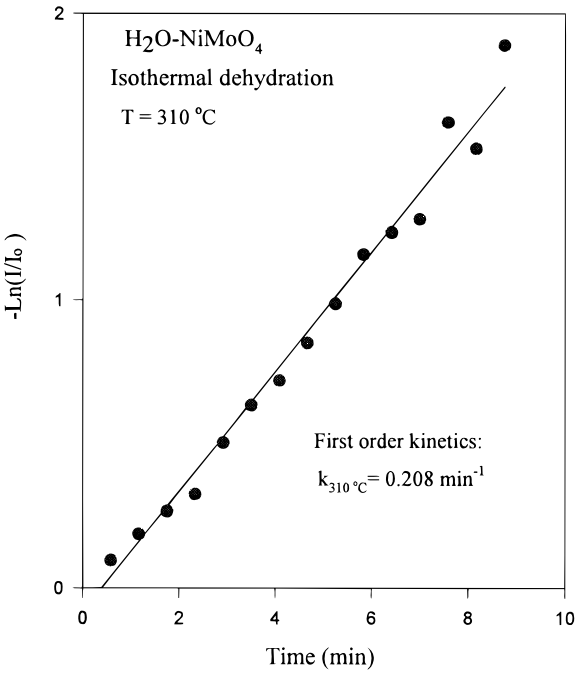

Figure 6. Logarithm of the concentration of $H_2O-NiMoO_4$ as a function of time at 310 °C. The concentration of $H_2O-NiMoO_4$ was assumed to be proportional to the intensity of the 2θ line at 18.3° in the XRD pattern ($\lambda = 0.957$ Å).

On the basis of these results we can assign the peaks in the H_2O-TDS spectra for $H_2O-NiMoO_4$ in Figure 1: the desorption features at 280−350 °C correspond to the evolution of water molecules that form an integral part of the crystal structure of $H_2O-NiMoO_4$, whereas the features at 120−160 and 490−530 °C are associated with the desorption of water molecules reversibly bound to the hydrate and the β-isomorph, respectively.

From the isothermal experiments in Figure 5 one can get the rate of disappearance of $H_2O-NiMoO_4$ at 310 °C. Figure 6 shows how the logarithm of the intensity of the 2θ line at 18.3° changes with time. The linear relationship between $\ln(I/I_o)$ and time indicates that the $H_2O-NiMoO_4 \rightarrow \beta$-$NiMoO_4$ transformation follows a kinetics of first order with a rate constant of 0.208 min^{-1} at 310 °C. A similar rate constant was obtained for the $H_2O-CoMoO_4 \rightarrow \beta$-$CoMoO_4$ process at 239 °C. The H_2O-TDS results in Figure 1 and the XRD data in Figures 3 and 5 show that the loss of water and appearance of the β-isomorph occur at lower temperature (50−70 °C) for $H_2O-CoMoO_4$ than for $H_2O-NiMoO_4$.

III.2. α-$NiMoO_4$ to β-$NiMoO_4$ Transformation. The catalytic properties of the α- and β-phases of $NiMoO_4$ have been the subject of a large number of studies in recent years.[5,7−9,12,15,34] In the literature, there are doubts about the exact temperature and the extent of the $\alpha \rightarrow \beta$ and $\beta \rightarrow \alpha$ phase transitions in $NiMoO_4$. Using time-resolved XRD, we investigated the kinetics of the α-$NiMoO_4 \rightarrow \beta$-$NiMoO_4$ transformation. A typical result is shown in Figure 7. In the experiments with temperature as a variable ($\Delta T = at$, $a = 1-8$ °C/min), the $\alpha \rightarrow \beta$ transformation was observed between 550 and 670 °C and its rate showed a strong dependence on the heating rate (a). We also monitored the transformation under isothermal conditions ($T = 550$, 595, 610, or 620 °C). Figure 8 shows kinetic parameters obtained by analyzing the changes that occurred in the 2θ line that appears at 10.8° in the diffraction pattern for α-$NiMoO_4$. The top panel of the figure shows how the logarithm of the intensity of the 10.8° line changes with time at 550 °C. At this temperature the rate of the $\alpha \rightarrow \beta$

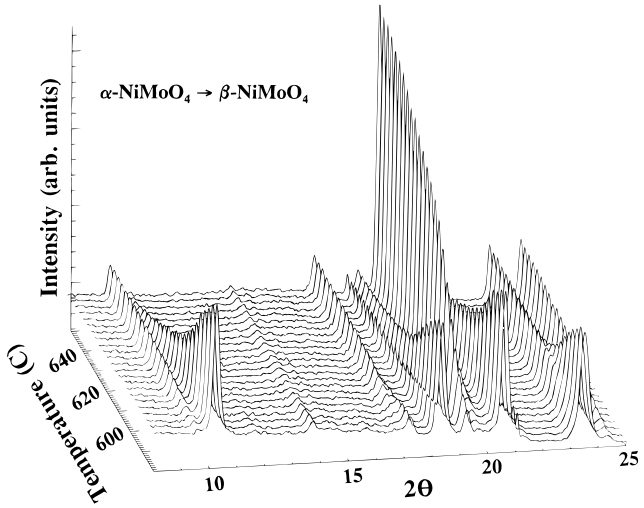

Figure 7. Time-resolved X-ray powder diffraction patterns for the α- to β-$NiMoO_4$ phase transition as a function of temperature. The experiments were carried out at a heating rate of 1.1 °C/min and using a wavelength of 1.116 Å.

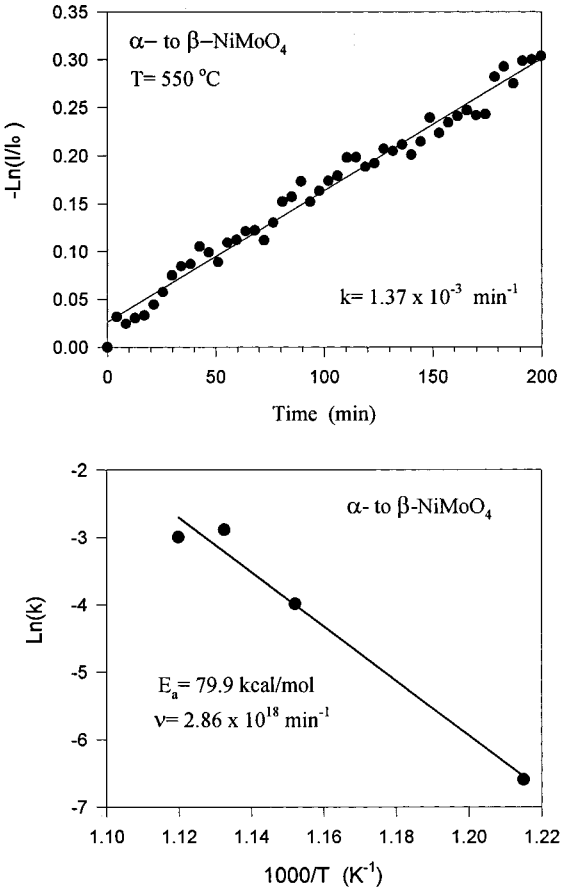

Figure 8. Top panel: Logarithm of the concentration of α-$NiMoO_4$ as a function of time at 550 °C. The concentration of α-$NiMoO_4$ was assumed to be proportional to the intensity of the 2θ line at 10.8° in the XRD pattern ($\lambda = 1.116$ Å). Bottom panel: Arrhenius plot for the transformation of α-$NiMoO_4$ into β-$NiMoO_4$.

transformation was very slow, and after 200 min only 27% of the α-phase had changed into the β-phase. The linear variation of $\ln(I/I_o)$ with time indicates that the $\alpha \rightarrow \beta$ transformation follows a kinetics of first order with a rate constant of 1.37×10^{-3} min^{-1}. The Arrhenius plot at the bottom of Figure 8 gives an apparent activation energy of 79.9 kcal/mol and a preexponential factor of 2.86×10^{18} min^{-1} for the phase transition.

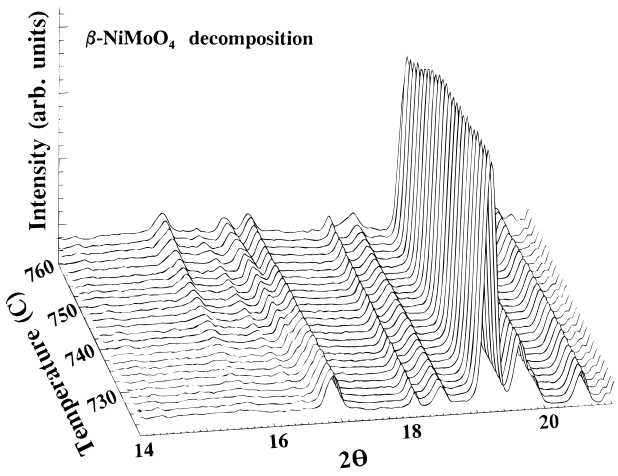

Figure 9. Decomposition of β-$NiMoO_4$ at high temperature. The time-resolved XRD experiments were carried out with a heating rate of 1.1 °C/min and using a wavelength of 1.116 Å.

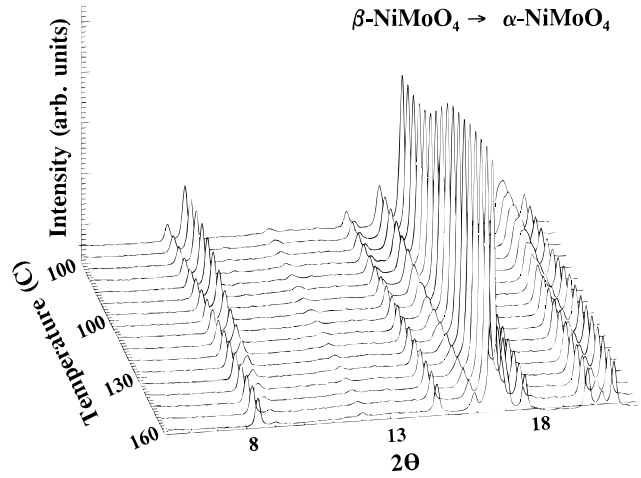

Figure 10. Time-resolved X-ray powder diffraction patterns for the β- to α-$NiMoO_4$ phase transition as a function of temperature. The sample was initially cooled from 500 to 100 °C at a cooling rate of 2 °C/min, then the temperature was held at 100 °C for 240 min. The XRD patterns were acquired using a wavelength of 0.957 Å.

The stability of β-$NiMoO_4$ as a function of temperature was examined using time-resolved XRD. The β-isomorph produced by heating $H_2O-NiMoO_4$ at 500 °C or α-$NiMoO_4$ at 650 °C was stable up to around 730 °C. At this temperature, extra lines appeared in the XRD patterns (see Figure 9). These new lines were very weak in intensity and can be attributed to nickel oxide left in the sample after the evaporation of MoO_3 at high temperature.[5,6] During the cooling of pure β-$NiMoO_4$ samples ($-\Delta T = 1-7$ °C/min), the onset of the $\beta \rightarrow \alpha$ phase transition appeared at 180−140 °C depending on the cooling rate. Typical results are shown in Figure 10. We found that the $\beta \rightarrow \alpha$ transformation did not follow the kinetics of first order as the $\alpha \rightarrow \beta$ transformation did. When cooling a pure β-$NiMoO_4$ sample, the final temperature had a critical effect in the amount of α-$NiMoO_4$ formed. For example, in the experiment of Figure 10, the rate of the $\beta \rightarrow \alpha$ transformation became negligible when the cooling was stopped at 100 °C. The system reached a metastable state and the variation in the relative amounts of the α and β phases was very small after holding the temperature at 100 °C for 240 min. A very large increase in the rate of α-$NiMoO_4$ formation was seen after dropping the temperature from 100 to 25 °C.

In a set of experiments, we studied the α-$CoMoO_4$ → β-$CoMoO_4$ transformation. This phase transition occurred at

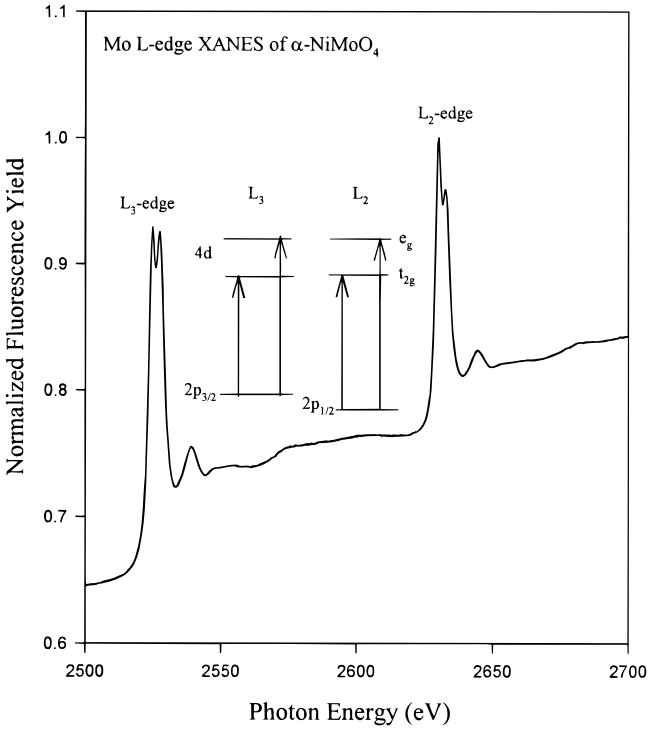

Figure 11. Mo $L_{2,3}$-edge fluorescence spectrum of α-$NiMoO_4$. In the center of the figure is shown the assignment of the white line features.

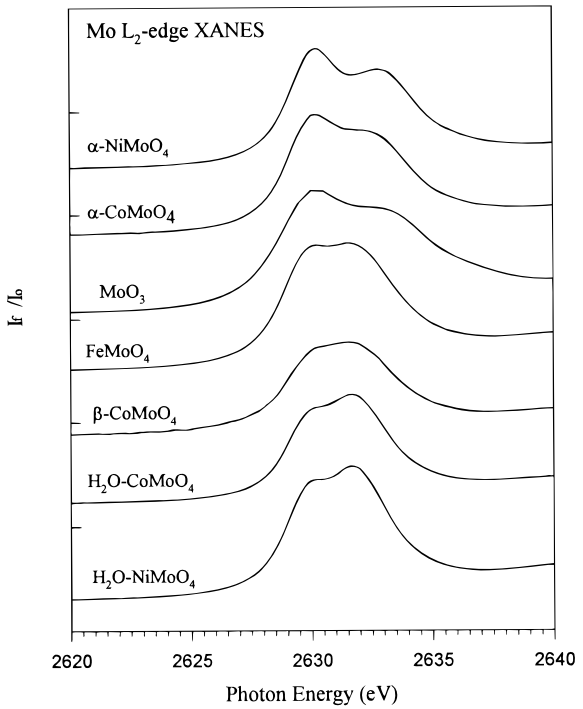

Figure 12. Mo L_2-edge XANES spectra for α-$NiMoO_4$, α-$CoMoO_4$, MoO_3, $FeMoO_4$, β-$CoMoO_4$, $H_2O-CoMoO_4$, and $H_2O-NiMoO_4$. All the spectra were recorded at room temperature.

temperatures between 330 and 410 °C, which are considerably smaller than those found for the α-$NiMoO_4$ → β-$NiMoO_4$ transformation. During the heating to high temperature of pure β-$CoMoO_4$, the onset for decomposition occurred around 760−780 °C (weak extra lines appeared in the XRD patterns at 12°−16°, $\lambda = 1.116$ Å). These temperatures are somewhat higher than those observed at the onset for the decomposition of β-$NiMoO_4$ (730−750 °C). After cooling the pure β-$CoMoO_4$ to 25 °C there was no formation of the corresponding α-isomorph. This is in contrast to the $\beta \rightarrow \alpha$ transformation seen in $NiMoO_4$. All these differences indicate that the β-phase of $NiMoO_4$ is less stable than that of $CoMoO_4$.

III.3. XANES of Cobalt and Nickel Molybdates. The local symmetry of the Mo atoms in molybdenum oxides can be determined using XANES at the Mo $L_{2,3}$-edges.[4,22] Figure 11 displays the Mo $L_{2,3}$-edge fluorescence spectrum of α-$NiMoO_4$. This spectroscopy probes 2p → 4d electronic transitions, and the splitting in the Mo $L_{2,3}$-edges reflects the ligand field splitting of the d orbitals:[4,22] e and t_2 in T_d symmetry; t_{2g} and e_g in O_h symmetry. In a tetrahedral coordination the splitting of the Mo 4d orbitals is smaller than the splitting in an octahedral coordination.[4,22] The most intense component of the split peak is at higher energy for tetrahedral compounds ($e < t_2$), whereas for octahedral coordination the most intense component occurs at lower energy ($t_{2g} < e_g$).[4,22] In Figure 11, the line shape and splitting of the peaks indicate that the Mo atoms are in an octahedral environment, in agreement with that found in XRD studies.[1−3]

Figure 12 shows Mo L_2-edge XANES spectra for a series of molybdates. In Table 1 are listed the corresponding "splittings" (measured simply as peak-to-peak separations) for the L_2 and L_3 edges of these compounds. In MoO_3, α-$NiMoO_4$ and α-$CoMoO_4$ the Mo atoms have an octahedral coordination and their $L_{2,3}$-edge spectra are very different from those of $H_2O-NiMoO_4$ and $H_2O-CoMoO_4$. The hydrates exhibit $L_{2,3}$-edge spectra similar to that of β-$CoMoO_4$ and those reported for molybdates in which the Mo atoms are in a tetrahedral coordination.[4,22] Thus, it appears that the Mo centers in $H_2O-NiMoO_4$ and $H_2O-CoMoO_4$ are under tetrahedral symmetry. Therefore, it is not surprising that upon losing water these compounds produce β-isomorphs in which the Mo atoms are also in a tetrahedral environment.[1−3] In a previous study it was found that the L_2-edge splitting for molybdenum oxides with Mo atoms in an almost perfect octahedral coordination was ∼4 eV.[4] The smaller splitting observed for α-$NiMoO_4$ and α-$CoMoO_4$ (2.7−3.1 eV) probably reflects the fact that in these compounds there is distortion in the octahedral angles and not all the Mo−O distances are equal.[1−3]

TABLE 1: Mo d Orbital Splitting from Mo $L_{2,3}$-edge XANES Spectra

compound	L_2-edge (eV)	L_3-edge (eV)
MoO_3	3.2 (O_h)	2.9 (O_h)
α-$NiMoO_4$	3.1 (O_h)	2.8 (O_h)
α-$CoMoO_4$	2.7 (O_h)	2.5 (O_h)
$FeMoO_4$	1.6 (T_d)	2.1 (T_d)
β-$CoMoO_4$	1.5 (T_d)	2.0 (T_d)
$H_2O-NiMoO_4$	1.6 (T_d)	2.1 (T_d)
$H_2O-CoMoO_4$	1.6 (T_d)	2.0 (T_d)

Now, we will shift our attention to the XANES results for the edges of the second metal in the molybdates. Figure 13 displays XANES spectra for the Co K-, L_2-, and L_3-edges of the Co molybdates. In the K-edge spectra (bottom panel in the figure), the pre-edge features are associated with Co(1s) → Co(3d) electronic transitions, whereas the edge primarily probes Co(1s) → Co(4p) transitions.[35,36] The magnitude of the 1s → 3d pre-edge transition has been used to determine the symmetry around the Co atoms in a large series of compounds.[36] This transition is symmetry forbidden in a strictly octahedral field but is allowed in a tetrahedral field.[35−37] In Figure 13 the Co K-edge spectrum for $CoAl_2O_4$, a compound in which Co is tetrahedrally coordinated to oxygen,[38] exhibits a clear pre-edge peak. No such a peak is seen in the Co K-edge spectra for the cobalt molybdates. This result indicates that the Co atoms in $H_2O-CoMoO_4$ are in an octahedral environment as the Co

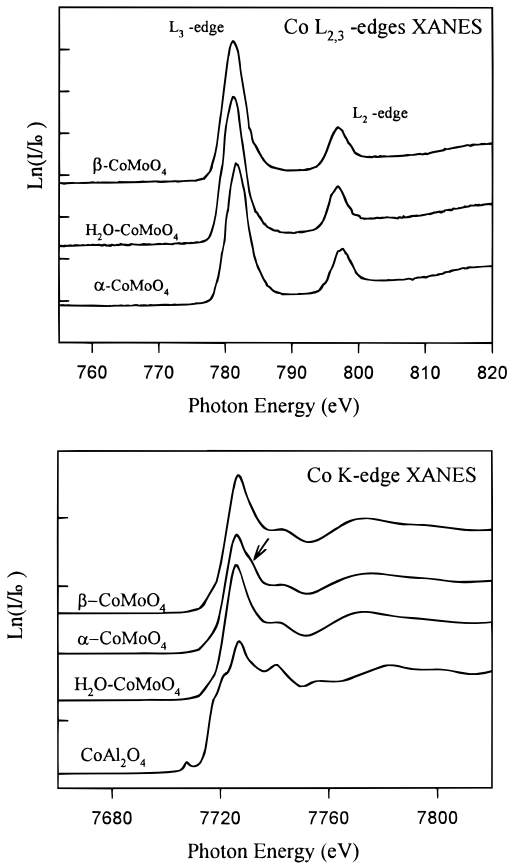

Figure 13. Co K-edge (bottom panel) and L-edge (top panel) XANES spectra for $H_2O-CoMoO_4$, α-$CoMoO_4$, β-$CoMoO_4$, and $CoAl_2O_4$. All the spectra were recorded at room temperature.

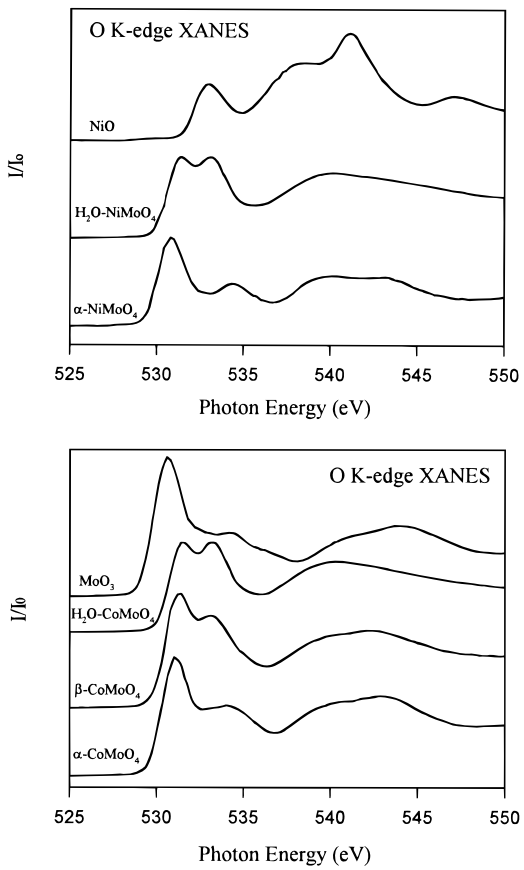

Figure 14. O K-edge XANES spectra for nickel (top panel) and cobalt (bottom panel) molybdates. For comparison the corresponding spectra for NiO and MoO_3 are also included. All the spectra were recorded at room temperature.

atoms in the α- and β-isomorphs.[1−3] Octahedral coordination is also expected for the Ni atoms of $H_2O-NiMoO_4$ and α-$NiMoO_4$, since the Ni K-edge spectra for these compounds do not show any pre-edge feature.[39] In Figure 13 the Co K-edge spectra of $H_2O-CoMoO_4$ and β-$CoMoO_4$ have a very similar line shape. On the other hand, the corresponding spectrum for α-$CoMoO_4$ exhibits a distinct feature ∼7 eV above the main peak (see arrow) that is not observed in the other cobalt molybdates. The same difference is found when comparing the Ni K-edge spectra of α-$NiMoO_4$ and $H_2O-NiMoO_4$.[39]

The top panel in Figure 13 shows Co $L_{2,3}$-edge XANES spectra for the cobalt molybdates. These edges reflect Co(2p) → Co(3d) electronic transitions. The Co L-edges of the molybdates are very similar. The only significant difference is in the position of the peaks, which are ∼0.4 eV at higher energy in α-$CoMoO_4$ than in $H_2O-CoMoO_4$ or β-$CoMoO_4$. A similar difference was observed in the Ni $L_{2,3}$-edge spectra of α-$NiMoO_4$ and $H_2O-NiMoO_4$.[39] The L-edge results indicate that the 3d orbitals of Co and Ni, which are involved in Co−O and Ni−O bonding, are under a similar chemical environment in all these compounds. In Figure 13, the Co L-edge spectra of the molybdates are very different from that reported for CoO,[40] a compound where Co is also in an octahedral coordination and has a formal oxidation state of +2. The Co L_3-edge XANES spectrum for CoO is characterized by four clear peaks (three of which are strong and have similar intensity) that appear in a window of 4 eV,[40] instead of one peak like the spectra in Figure 13 (which have a line shape that does not match well the convolution of the peaks for CoO). The ground state of CoO has been described as a high-spin $3d^7$ configuration with $^4T_1$ symmetry.[40a] The peaks in the L-edge spectrum of CoO probably come from a multiplet of states associated with $3d^7[^4T_1] \rightarrow 2p^53d^8$ transitions.[40a,41] In the case of the cobalt molybdates, the Co atoms could be in a low spin $3d^7$ configuration which would lead to a reduced number of peaks in the Co L-edge spectrum.[41] Low spin configurations have been detected in the Co $L_{2,3}$-edge XANES spectra for $LaCoO_3$[42] and $LiCoO_2$.[40b]

Figure 14 displays O K-edge spectra for the cobalt and nickel molybdates. For transition metal oxides, a direct relation has been found between the features in the O K-edge spectrum and the number of d electrons in the metal.[23,26] The structures at the O K-edge arise from covalent mixing of the metal and oxygen states, which introduces O(2p) character in unoccupied states of mainly metal character making the O(1s) → metal-(d,s,p) electronic transitions dipole allowed.[23,26] In general, the O K-edge XANES spectra of oxides can be divided in two regions.[23,26] The first is a double-peaked sharp structure near the threshold which is related to O(1s) → metal(d) transitions. This is followed by a second region that has a broad structure 5−10 eV above the edge and comes from O(1s) → metal(s,p) transitions.

The case of the cobalt and nickel molybdates is particularly interesting because these oxides contain two different metals. In principle, one can have electron transfer from the O 1s orbitals into the empty orbitals of both metals. In Figure 14, the O K-edge spectra of the molybdates have line shapes that are very different from those seen in the corresponding spectra of NiO[23,26] and CoO,[40a] but similar to that found for the O K-edge spectrum of MoO_3. This indicates that the O 1s electrons are mainly excited into the empty Mo(4d,5s,5p) orbitals. Three phenomena may be responsible for this behavior. First, the O(1s) → Mo-

TABLE 2: First-to-Second Peak Separation in O K-edge XANES Spectra

compound	splitting (eV)	Mo symmetry
MoO_3	3.4	O_h
α-$NiMoO_4$	3.6	O_h
α-$CoMoO_4$	3.2	O_h
$FeMoO_4$	1.8	T_d
β-$CoMoO_4$	1.9	T_d
$H_2O-NiMoO_4$	1.7	T_d
$H_2O-CoMoO_4$	1.7	T_d

(4d,5s,5p) transitions may occur at lower energy than O(1s) → Ni(3d,4s,4p) or O(1s) → Co(3d,4s,4p) transitions. Second, the mixing of the O(2p) orbitals with the Mo(4d) orbitals is probably stronger than with the 3d orbitals of Co or Ni, making the O(1s) → metal(d) transition more dipole allowed in the case of Mo. And third, Mo^{6+} has a fully empty valence d shell, while the valence d shells of Co^{2+} and Ni^{2+} are more than half occupied. In Figure 14, one can see a large change in the line shape of the two peaks near the threshold (0−5 eV) when the local symmetry of the Mo atoms changes from octahedral to tetrahedral. In MoO_3, α-$CoMoO_4$, and α-$NiMoO_4$ (O_h symmetry), the first peak is twice more intense than the second. In the case of β-$CoMoO_4$, $H_2O-CoMoO_4$, and $H_2O-NiMoO_4$ (T_d symmetry), the second peak gains intensity with respect to the first. These trends match very well those observed for the Mo(2p) → Mo(4d) transitions in the Mo $L_{2,3}$-edge spectra of Figure 12, and also can be explained by taking into consideration the relative energy of the Mo 4d orbitals in octahedral ($t_{2g} < e_g$) and tetrahedral ($e < t_2$) fields. Furthermore, the changes in the separation between the first and second peak in the O K-edge spectra also track very well variations in the splitting of the Mo L_2- and L_3-edges, as can be seen by comparing the values listed in Tables 1 and 2. The trends in both sets of data reflect changes in the magnitude of the t_2-e splitting when going from octahedral to tetrahedral coordination. The XANES results in Figure 14 suggest that the O K-edge features can be very useful for probing the local symmetry of Mo atoms in molybdenum oxides.

IV. Discussion

IV.1. Properties of $H_2O-CoMoO_4$ and $H_2O-NiMoO_4$. The results of XANES for the hydrates of $CoMoO_4$ and $NiMoO_4$ (general formula $AMoO_4 \cdot nH_2O$[7]) indicate that in these compounds Co and Ni have octahedral coordination, while Mo exhibits tetrahedral coordination. This structural configuration is identical to that observed for the corresponding β-isomorphs.[1−3] Previously, on the basis of results of differential thermal analysis,[16] it was suggested that in $H_2O-NiMoO_4$ and β-$NiMoO_4$ the coordination of Mo is similar.[7] In studies for hydrates of manganese molybdates ($MnMoO_4 \cdot nH_2O$) several X-ray powder patterns have been found.[43] One crystal structure contains Mo^{6+} tetrahedra and Mn^{2+} octahedra.[43]

The H_2O-TDS results in Figure 1 show two strong desorption peaks for water at temperatures below 500 °C. Thermal desorption spectra for the $NiMoO_4 \cdot {}^3/_4H_2O \cdot {}^3/_4NH_3$ compound show desorption of water between 100 and 200 °C and desorption of ammonia from 200 to 400 °C.[34] The formation of β-$NiMoO_4$ is only observed after the desorption of NH_3.[34] This behavior resembles that found in our experiments for $H_2O-NiMoO_4$, where β-$NiMoO_4$ appears after the desorption of water at temperatures between 200 and 400 °C. Thus, when going from $NiMoO_4 \cdot {}^3/_4H_2O \cdot {}^3/_4NH_3$ to $NiMoO_4 \cdot nH_2O$, one replaces NH_3 with H_2O in the crystal structure of the compound. The stability of these molecules in the lattice is very similar, and the $NiMoO_4 \cdot {}^3/_4H_2O \cdot {}^3/_4NH_3$ and $NiMoO_4 \cdot nH_2O$ precursors produce β-$NiMoO_4$ at similar temperatures.

The results of time-resolved XRD experiments indicate that the $H_2O-AMoO_4$ → β-$AMoO_4$ + H_2O reaction follows a kinetics of first order. Both hydrates transform directly into the β-isomorph without any intermediate phase. This is probably facilitated by the similarities that $H_2O-AMoO_4$ and β-$AMoO_4$ have in their structural and electronic properties. The relatively low temperatures at which the $H_2O-AMoO_4$ → β-$AMoO_4$ + H_2O process occurs (240−340 °C) make the hydrates very good precursors for the preparation of β-$AMoO_4$ catalysts used in the partial oxidation of hydrocarbons.[8,15] It has been found that $H_2O-AMoO_4$ is a better precursor for HDS catalysts than α-$AMoO_4$ or β-$AMoO_4$ synthesized by calcination at 760 °C.[7,19] This seems to be related to the in situ generation of β-$AMoO_4$ during the activation of the hydrate at 400 °C.[7]

IV.2. Properties of the α and β Phases of $CoMoO_4$ and $NiMoO_4$. The time-resolved XRD experiments for the cobalt and nickel molybdates indicate that the α → β transformations occur at considerably higher temperatures than the hydrate → β transformations (∼150 °C in $CoMoO_4$ and 280 °C in $NiMoO_4$). For similar heating rates, the former transformations cover temperature ranges (70−100 °C) that are longer than those necessary for the completion of the latter transformations (20−50 °C). The activation energy for the α-$NiMoO_4$ → β-$NiMoO_4$ transition is ∼40 kcal/mol higher than that for the $H_2O-NiMoO_4$ → β-$NiMoO_4$ + H_2O reaction. These differences probably reflect the fact that the hydrate → β transformation does not produce a change in the coordination of the metal atoms, whereas the α → β transformation involves a change in the coordination of Mo (O_h → T_d).

When comparing the behavior of the cobalt and nickel molybdates, one finds that the α → β and hydrate → β transformations take place at a lower temperature in the case of $CoMoO_4$. During the heating of the pure β-isomorphs to high temperature, the onset for the decomposition of β-$NiMoO_4$ is ∼40 °C smaller than the onset for the decomposition of β-$CoMoO_4$. Upon cooling to room temperature, β-$NiMoO_4$ transforms into α-$NiMoO_4$, while no transformation is seen for β-$NiMoO_4$. All these differences in behavior indicate that the β-phase of $CoMoO_4$ is substantially more stable than that of $NiMoO_4$. This explains why it is much easier to reduce β-$NiMoO_4$ than β-$CoMoO_4$ in H_2-TPR experiments.[7] In previous studies, it was found that β-$NiMoO_4$ is a better precursor for active HDS catalysts than β-$CoMoO_4$.[7] During the generation of the active catalysts, Mo−O bonds are replaced with Mo−S bonds.[7] The higher stability of β-$CoMoO_4$ probably makes more difficult the sulfidation of this molybdate and the subsequent formation of active sites for the HDS process.

The K- and L-edges of Co indicate that there are no major changes in the electronic properties of this metal when going from α-$CoMoO_4$ to β-$CoMoO_4$. The $L_{2,3}$-edges of Mo and the K-edge of O show large variations in the electronic properties of Mo as the coordination of the metal varies from octahedral to tetrahedral in the cobalt and nickel molybdates. These changes in the electronic properties of Mo correlate with changes in the catalytic activity of the α- and β-isomorphs.[5,7,15] The β-phase of $NiMoO_4$ is almost twice as selective for the dehydrogenation of propane to propene than the α-phase.[15] In a similar way, the sulfided β-$AMoO_4$ compounds were found to be much better catalysts for the HDS of thiophene than the sulfided α-isomorphs.[5,7] In the tetrahedral environment of the β-phase, a Mo^{6+} ion is coordinatively unsaturated and in overall its empty 4d orbitals are less destabilized than in an octahedral

field.[44] This could favor bonding interactions between the Mo 4d orbitals and the occupied orbitals of hydrocarbons or the sulfur lone pairs of thiols and sulfides, making the β-phase more chemically active than the α-phase.

V. Conclusions

1. Upon heating $H_2O-AMoO_4$ (A = Co or Ni) to high temperature in TDS experiments, water desorbs in two peaks. The first one appears at 100−200 °C and is associated with water molecules reversible bound to the hydrate. The second peak appears from 200 to 400 °C and corresponds to the desorption of water molecules that form part of the crystal structure of the hydrate. At the onset of this peak, the formation of β-$AMoO_4$ starts. The $H_2O-AMoO_4 \rightarrow \beta$-$AMoO_4 + H_2O$ reaction follows a kinetics of first order.

2. The α-$NiMoO_4 \rightarrow \beta$-$NiMoO_4$ transformation takes place between 550 and 670 °C and its rate follows a kinetics of first order with an apparent activation energy of 79.9 kcal/mol and a preexponential factor of 2.86×10^{18} min^{-1}. β-$NiMoO_4$ decomposes at temperatures above 730 °C and transforms into α-$NiMoO_4$ at temperatures below 180 °C. In the case of $CoMoO_4$, the $\alpha \rightarrow \beta$ transition occurs between 330 and 410 °C. Above 760 °C the decomposition of β-$CoMoO_4$ begins, and no formation of α-$CoMoO_4$ was seen after cooling β-$CoMoO_4$ to room temperature. β-$CoMoO_4$ is more stable than β-$NiMoO_4$.

3. The results of XANES for the hydrates of $CoMoO_4$ and $NiMoO_4$ indicate that in these compounds, Co and Ni have octahedral coordination, while Mo exhibits tetrahedral coordination. This structural configuration is identical to that observed for the corresponding β-isomorphs.

4. The K- and L-edges of Co indicate that there are no big variations in the electronic properties of this metal when comparing $H_2O-CoMoO_4$, α-$CoMoO_4$, and β-$CoMoO_4$. The same is valid for the electronic properties of Ni in the nickel molybdates. On the other hand, the $L_{2,3}$-edges of Mo show large changes in the splitting of the Mo 4d orbitals as the coordination of this metal varies from octahedral in the α-isomorphs to tetrahedral in the β-isomorphs and hydrates. The features near the threshold in the O K-edge spectra track very well the splitting of the Mo 4d orbitals in tetrahedral and octahedral fields and can be very useful for probing the local symmetry of Mo atoms in molybdenum oxides.

Acknowledgment. The authors thank D. A. Fischer and F.-L. Lu for their help with the use of the U7A and X19A beamlines, respectively, at the NSLS. The NSLS is supported by the Divisions of Materials and Chemical Sciences of the U.S. Department of Energy. The work carried out at the Chemistry Department of BNL was supported under contract DE-AC02-76CH00016 with the U.S. Department of Energy, Office of Basic Energy Sciences, Chemical Science Division. J.L.B. gratefully acknowledges a grant from ACS that made possible a visit to BNL.

References and Notes

(1) Smith, G. W.; Ibers, J. A. *Acta Crystallogr.* **1965**, *19*, 269.
(2) Smith, G. W. *Acta Crystallogr.* **1962**, *15*, 1054.
(3) Sleight, A. W.; Chamberland, B. L. *Inorg. Chem.* **1968**, *7*, 1673.
(4) Bare, S. R.; Mitchell, G. E.; Maj, J. J.; Vrieland, G. E.; Gland, J. L. *J. Phys. Chem.* **1993**, *97*, 6048.
(5) Brito, J. L.; Barbosa, A. L.; Albornoz, A.; Severino, F.; Laine, J. *Catal. Lett.* **1994**, *26*, 329.
(6) Brito, J. L.; Laine, J.; Pratt, K. C. *J. Mater. Sci.* **1989**, *24*, 425.
(7) Brito, J. L.; Barbosa, A. L. *J. Catal.* **1997**, *171*, 467.
(8) Zou, J.; Shrader, G. L. *J. Catal.* **1996**, *161*, 667.
(9) Madeira, L. M.; Maldonado-Hodar, F. J.; Portela, M. F.; Freire, F.; Martin-Aranda, R. M.; Oliveira, M. *Appl. Catal. A: Gen.* **1996**, *135*, 137.
(10) Dunne, S. J.; Burns, R. C.; Lawrance, G. A. *Aust. J. Chem.* **1992**, *45*, 1943.
(11) Brito, J. L.; Laine, J. *Appl. Catal.* **1991**, *72*, L13, and references therein.
(12) Martin-Aranda, R. M.; Portela, M. F.; Madeira, L. M.; Freire, F.; Oliveira, M. *Appl. Catal. A: Gen.* **1995**, *127*, 201.
(13) Kapoor, R.; Oyama, S. T.; Fruhberger, B.; Chen, J. G. *J. Phys. Chem.* **1997**, *101*, 1543.
(14) (a) Di Renzo, F.; Mazzocchia, C.; Thomas, G.; Vernay, A. M. *React. Solids* **1988**, *6*, 145. (b) Mazzocchia, C.; Di Renzo, F.; Aboumrad, C.; Thomas, G. *Solid State Ionics* **1989**, *32/33*, 228.
(15) Mazzocchia, C.; Aboumrad, C.; Diagne, C.; Tempesti, E.; Herrmann, J. M.; Thomas, G. *Catal. Lett.* **1991**, *10*, 181.
(16) Di Renzo, F.; Mazzocchia, C. *Thermochim. Acta* **1985**, *85* 139.
(17) (a) Doyle, W. P.; McGuire, G.; Clark, G. M. *J. Inorg. Nucl. Chem.* **1966**, *28*, 1185. (b) Rajaram, P.; Vismanathan, B.; Aravamudan, G.; Srinivasan, V.; Sastri, M. V. C. *Thermochim. Acta* **1973**, *7*, 123.
(18) Mazzocchia, C.; Di Renzo, F.; Centola, P. *Rev. Port. Quim.* **1977**, *19*, 61.
(19) Laine, J.; Pratt, K. C. *React. Kinet. Catal. Lett.* **1979**, **10**, 207.
(20) Madeley, R. A.; Wanke, S. *Appl. Catal.* **1988**, *39*, 295.
(21) Hu, H.; Wachs, I. E.; Bare, S. R. *J. Phys. Chem.* **1995**, *99*, 10897.
(22) Hedman, B.; Penner-Hahn, J. E.; Hodgson, K. O. In *EXAFS and Near Edge Structure III*; Hodgson, K. O., Hedman, B., Penner-Hahn, J. E., Eds.; Springer-Verlag: Berlin, 1984.
(23) Chen, J. G.; Fruhberger, B.; Colaianni, M. L. *J. Vac. Sci. Technol. A* **1996**, *14*, 1668.
(24) Chen, J. G. *Surf. Sci. Rep.* **1997**, *30*, 1.
(25) Hrbek, J.; Sham, T. K.; Shek, M.-L.; Xu, G.-Q. *Langmuir* **1992**, *8*, 2461.
(26) (a) Grunes, L. A.; Leapman, R. D.; Wilker, C. N.; Hoffmann, R.; Kunz, A. B. *Phys. Rev. B* **1982**, *25*, 7157. (b) de Groot, F. M. F.; Grioni, M.; Fuggle, J. C.; Ghijsen, J.; Sawatzky, G. A.; Petersen, H. *Phys. Rev. B* **1989**, *40*, 5715.
(27) (a) Norby, P.; Christensen, A. N.; Hanson, J. C. *Stud. Surf. Sci. Catal.* **1994**, *84*, 179. (b) Nørlund-Christensen, A.; Norby, P.; Hanson, J. C. *J. Solid State Chem.* **1995**, *114*, 556. (c) Grey, C. P.; Poshni, F. I.; Gualtieri, A. F.; Norby, P.; Hanson, J. C.; Corbin, D. R. *J. Am. Chem. Soc.* **1997**, *119*, 1981. (d) Norby, P.; Hanson, J. *Catal. Today*, submitted for publication.
(28) Hastings, J. B.; Suortii, P.; Thomsolin, P.; Kvick, A.; Koetzle, T. *Nucl. Instrum. Methods* **1983**, *208*, 55.
(29) Gualtieri, A.; Norby, P.; Artioli, G.; Hanson, J. *Phys. Chem. Miner.* **1997**, *24*, 191.
(30) (a) Stern, E.; Heald, S. *Rev. Sci. Intrum.* **1979**, *50*, 1579. (b) Lytle, F. W.; Greegor, R. B.; Sandstrom, D. R.; Marques, E. C.; Wong, J.; Spiro, C. L.; Huffman, G. P.; Huggins, F. E. *Nucl. Instrum. Methods Phys. Res.* **1984**, *226*, 542.
(31) Fischer, D. A., manuscript in preparation.
(32) JCPDS Powder Diffraction File, Int. Center for Diffraction Data, Swarthmore, PA, 1989.
(33) (a) Haber, *J. Less-Common Metals* **1974**, *36*, 277. (b) Plyasova, L. M.; Karakchiev, L. G. *Inorg. Mater.* (*Engl. Transl.*) **1972**, *100*, 100.
(34) Mazzocchia, C.; Anouchinsky, R.; Kaddouri, A.; Sautel, M.; Thomas, G. *J. Thermal Anal.* **1993**, *40*, 1253.
(35) Shulman, R. G.; Yafet, Y.; Eisenberger, P.; Blumberg, W. E. *Proc. Natl. Acad. Sci. U.S.A.* **1976**, *73*, 1384.
(36) Barrett, P. A.; Sankar, G.; Catlow, C. R. A.; Thomas, J. M. *J. Phys. Chem.* **1996**, *100*, 8977, and references therein.
(37) Chiu, N.-S.; Bauer, S. H.; Johnson, M. F. L. *J. Catal.* **1984**, *89*, 226.
(38) Toriuma, K.; Ozima, M.; Akaogi, M.; Sato, Y. *Acta Crystallogr. B* **1978**, *34*, 1093.
(39) Chaturvedi, S.; Rodriguez, J. A.; Hanson, J. C.; Brito, J. L.; Lee, P., manuscript in preparation.
(40) (a) de Groot, F. M. F.; Abbate, M.; van Elp, J.; Sawatzky, G. A.; Ma, Y. J.; Chen, C. T.; Sette, F. *J. Phys: Condens. Matter* **1993**, *5*, 2277. (b) van Elp, J.; Wieland, J. L.; Eskes, H.; Kuiper, P.; Sawatzky, G. A.; de Groot, F. M. F.; Turner, T. S. *Phys. Rev.* B **1991**, *44*, 6090.
(41) (a) Huheey, J. E. *Inorganic Chemistry*, 3rd ed.; Harper & Row: New York, 1983; pp 449−450. (b) Gray, H. B. *Electrons and Chemical Bonding*; Benjamin: New York, 1965; pp 200−201.
(42) Abbate, M.; Fuggle, J. C.; Fujimori, A.; Tjeng, L. H.; Chen, C. T.; Potze, R.; Sawatzky, G. A.; Eisaki, H.; Uchida, S. *Phys. Rev. B* **1993**, *47*, 16124.
(43) Clearfield, A.; Moini, A.; Rudolf, P. R. *Inorg. Chem.* **1985**, *24*, 4606, and references therein.
(44) See pages 377 and 378 in ref 41a.